Magnetic field annihilation and reconnection driven by femtosecond lasers in inhomogeneous plasma

Wang YouYuan, Li FeiYu, Chen Min, Weng SuMing, Lu QuanMing, Dong QuanLi, Sheng ZhengMing and Zhang Jie

Citation: SCIENCE CHINA Physics, Mechanics & Astronomy **60**, 115211 (2017); doi: 10.1007/s11433-017-9086-9

View online: http://engine.scichina.com/doi/10.1007/s11433-017-9086-9

View Table of Contents:http://engine.scichina.com/publisher/scp/journal/SCPMA/60/11

Published by the Science China Press

SCIENCE CHINA
Physics, Mechanics & Astronomy

CrossMark click for updates

• Article •

November 2017 Vol. 60 No. 11: 115211
doi: 10.1007/s11433-017-9086-9

Magnetic field annihilation and reconnection driven by femtosecond lasers in inhomogeneous plasma

YouYuan Wang[1,2], FeiYu Li[3], Min Chen[1,2], SuMing Weng[1,2], QuanMing Lu[4], QuanLi Dong[2,5], ZhengMing Sheng[1,2,3*], and Jie Zhang[1,2]

[1] *Key Laboratory for Laser Plasmas (Ministry of Education) and School of Physics and Astronomy, Shanghai Jiao Tong University, Shanghai 200240, China;*
[2] *Collaborative Innovation Center of IFSA (CICIFSA), Shanghai Jiao Tong University, Shanghai 200240, China;*
[3] *Scottish Universities Physics Alliance (SUPA), Department of Physics, University of Strathclyde, Glasgow G4 0NG, UK;*
[4] *Key Lab of Geospace Environment, Chinese Academy of Sciences, Department of Geophysics and Planetary Science, University of Science and Technology of China, Hefei 230026, China;*
[5] *School of Physics and Optoelectronic Engineering, Ludong University, Yantai 264025, China*

Received June 2, 2017; accepted July 21, 2017; published online August 18, 2017

The process of fast magnetic reconnection driven by intense ultra-short laser pulses in underdense plasma is investigated by particle-in-cell simulations. In the wakefield of such laser pulses, quasi-static magnetic fields at a few mega-Gauss are generated due to nonvanishing cross product $\nabla(n/\gamma)\times p$. Excited in an inhomogeneous plasma of decreasing density, the quasi-static magnetic field structure is shown to drift quickly both in lateral and longitudinal directions. When two parallel-propagating laser pulses with close focal spot separation are used, such field drifts can develop into magnetic reconnection (annihilation) in their overlapping region, resulting in the conversion of magnetic energy to kinetic energy of particles. The reconnection rate is found to be much higher than the value obtained in the Hall magnetic reconnection model. Our work proposes a potential way to study magnetic reconnection-related physics with short-pulse lasers of terawatt peak power only.

magnetic reconnection, laser wakefield, magnetic field generation

PACS number(s): 47.75.+f, 52.35.-g, 52.65.-y, 98.70.Sa

Citation: Y. Y. Wang, F. Y. Li, M. Chen, S. M. Weng, Q. M. Lu, Q. L. Dong, Z. M. Sheng, and J. Zhang, Magnetic field annihilation and reconnection driven by femtosecond lasers in inhomogeneous plasma , Sci. China-Phys. Mech. Astron. **60**, 115211 (2017), doi: 10.1007/s11433-017-9086-9

1 Introduction

Magnetic reconnection (MR) is a process by which oppositely directed magnetic field lines squeeze each other and reconnect, converting magnetic energy into particles' kinetic energy [1-3]. It is widely believed to play a key role in many explosive plasma phenomena, such as solar flares, fusion plasma instabilities, and laser-driven plasma jets [4-7]. Since 2007, laboratory study of MR-related processes by use of high-power, laser-produced plasma [2,7-8] and other plasma devices [9] has drawn increasing interest. For MR in laser-produced plasma, most experimental and numerical investigations have been carried out with nanosecond kJ-level high-energy lasers [6-8,10], where the magnetic fields are produced via the Biermann battery process due to nonparallel temperature and density gradients [11,12]. The involved magnetic fields are normally located near the target

*Corresponding author (email: zmsheng@sjtu.edu.cn)

surface, typically at the mega-Gauss (MG) level. Significant progress has been made in this field [13]. For example, three well-collimated high-speed electron jets were experimentally observed in the fanlike outflow region [6,14] to be consistent with the signatures of MR simulations [15]. Fully kinetic particle simulations showed that fast reconnection in these strongly driven systems can be explained by magnetic flux pileup at the shoulder of the current sheet [16]. However, most of the simulations did not include the laser-plasma interaction stages, simply by assuming that two bubbles with high energy electron currents start to evolve in a background plasma.

With the development of ultrashort high-power laser technologies, petawatt lasers with picosecond to femtosecond durations are now available. This makes it possible to investigate fast magnetic-field generation and dissipation under even higher quasi-static magnetic fields over 100 MGs by the relativistic intense lasers interaction with plasmas [2,16-18] or by the interaction of high current relativistic electron beams with plasmas [19,20].

In this paper, we report particle-in-cell (PIC) simulations of the MR process driven by intense femtosecond laser in inhomogeneous plasma. The idea is to send two parallel-propagating femtosecond laser pulses into a nonuniform layer of underdense plasma. High quasi-static magnetic fields are generated in the wakefield behind the pulses due to nonvanishing cross product [21] $\nabla(n/\gamma)\times\boldsymbol{p}$, where n is the electron density; $\boldsymbol{p}$ is the electron fluid momentum; and γ is the corresponding relativistic factor. The down-ramp density inhomogeneity causes lateral drift of the generated magnetic fields [22,23]. As a result, reconnection occurs when the magnetic fields having different polarities drift toward each other and become partly overlapped. This process can induce substantial electrostatic fields which accelerate charged particles and cause plasma heating. Prominently, such a setup features an ultra-fast reconnection rate, typically at the time scale of a few hundred femtoseconds.

2 Quasi-static magnetic field generation and drift

It is well known that large-amplitude plasma waves can be excited by an ultra-short intense laser pulse in underdense plasma. The wakefield can be as high as 1 GV/cm and can move with a phase velocity close to the group velocity of the laser pulse, making it ideal for compact particle acceleration [24,25]. In addition, quasi-static magnetic fields are produced due to wakefield excitation. By "quasi-static", we mean the magnetic fields evolve with a time scale much longer than the laser oscillation period. The equation for magnetic field generation in the laser wakefield can be described by the following general equation [21]:

$$\left(\nabla^2-\frac{1}{c^2}\frac{\partial^2}{\partial t^2}-\frac{n}{\gamma}\frac{\omega_p^2}{c^2}\right)\boldsymbol{B}=\frac{\omega_p}{c}\nabla\left(\frac{n}{\gamma}\right)\times\boldsymbol{p}, \tag{1}$$

where $\omega_p^2=n_0e^2/\epsilon_0 m_e$; the magnetic field $|\boldsymbol{B}|$ is normalized by $m_e\omega_p/e$; the density n is normalized by n_0 (the initial plasma density); the electron fluid momentum $|\boldsymbol{p}|$ is normalized by m_ec; and γ is the relativistic factor of the electron fluid. The nonvanishing cross product or the source term on the right-hand side of eq. (1) $\boldsymbol{S}=\nabla(n/\gamma)\times\boldsymbol{p}$ is responsible for the magnetic field generation. In homogeneous underdense plasma, eq. (1) can be simplified to

$$\left(\nabla_\perp^2-\frac{n}{\gamma}\frac{\omega_p^2}{c^2}\right)\boldsymbol{B}=\frac{\omega_p}{c}\nabla\left(\frac{n}{\gamma}\right)\times\boldsymbol{p}. \tag{2}$$

The source term points to the azimuthal direction in 3D geometry, as the laser pulse drives a net electric current to the opposite of the laser propagation direction. The scaling of the magnetic field strength with the driving laser intensity has been obtained as $|B|\propto I_{\rm L}^2$ under weakly relativistic laser intensity $I_{\rm L}$ and $|B|\propto I_{\rm L}$ for highly relativistic laser intensity [21]. It has also been shown that the magnetic field profile produced in homogeneous plasmas changes little up to the time scale of ion motion. Fast evolutions on the scale of electron motion are, however, anticipated in inhomogeneous plasmas by several theory models [22,23]. In particular, being excited along a down-ramp density profile, the magnetic field tends to rapidly drift along transverse and longitudinal directions. In the following, we carry out particle-in-cell (PIC) simulations with the code OSIRIS [26] to study the field evolutions and identify possible consequences of magnetic reconnection when two parallel-propagating laser pulses with close focal spot separations are sent to the plasma.

We begin with 2D PIC simulations, which although described in a simplified slab geometry can capture the key features of the present problem and can provide a reference for the further 3D simulation shown later. Figure 1(a) shows the simulation box, which is respectively 115 and 60 μm long in the X and Y directions. An underdense plasma consisting of electrons and protons is initialized in $0<X<85$ μm. While the transverse density is uniform, the longitudinal density profile is given by the green curve in Figure 1(a), i.e., $n_0=0.01n_{\rm c}$ in $0<X<30$ μm , then decreases as $n=n_0[1-\sin(\pi(x-30)/100)]$, in 30 μm $<X<70$ μm, and then remains constant again in 70 μm $<X<85$ μm, where $n_{\rm c}$ is the critical density. A linearly polarized laser pulse polarized along the Z direction and with the wavelength $\lambda_{\rm L}=1.0$ μm is incident along the X direction from the left boundary. It has a focal spot radius $w_0=4.0$ μm and pulse duration $\tau=13T_0=40$ fs, where $T_0=\lambda_{\rm L}/c\approx3.3$ fs. The normalized laser electric field is $a_0=eE_0/m_e\omega_0c=1.0$, where E_0 is the peak amplitude of the laser electric field and ω_0 is the laser frequency. It is related to the laser intensity

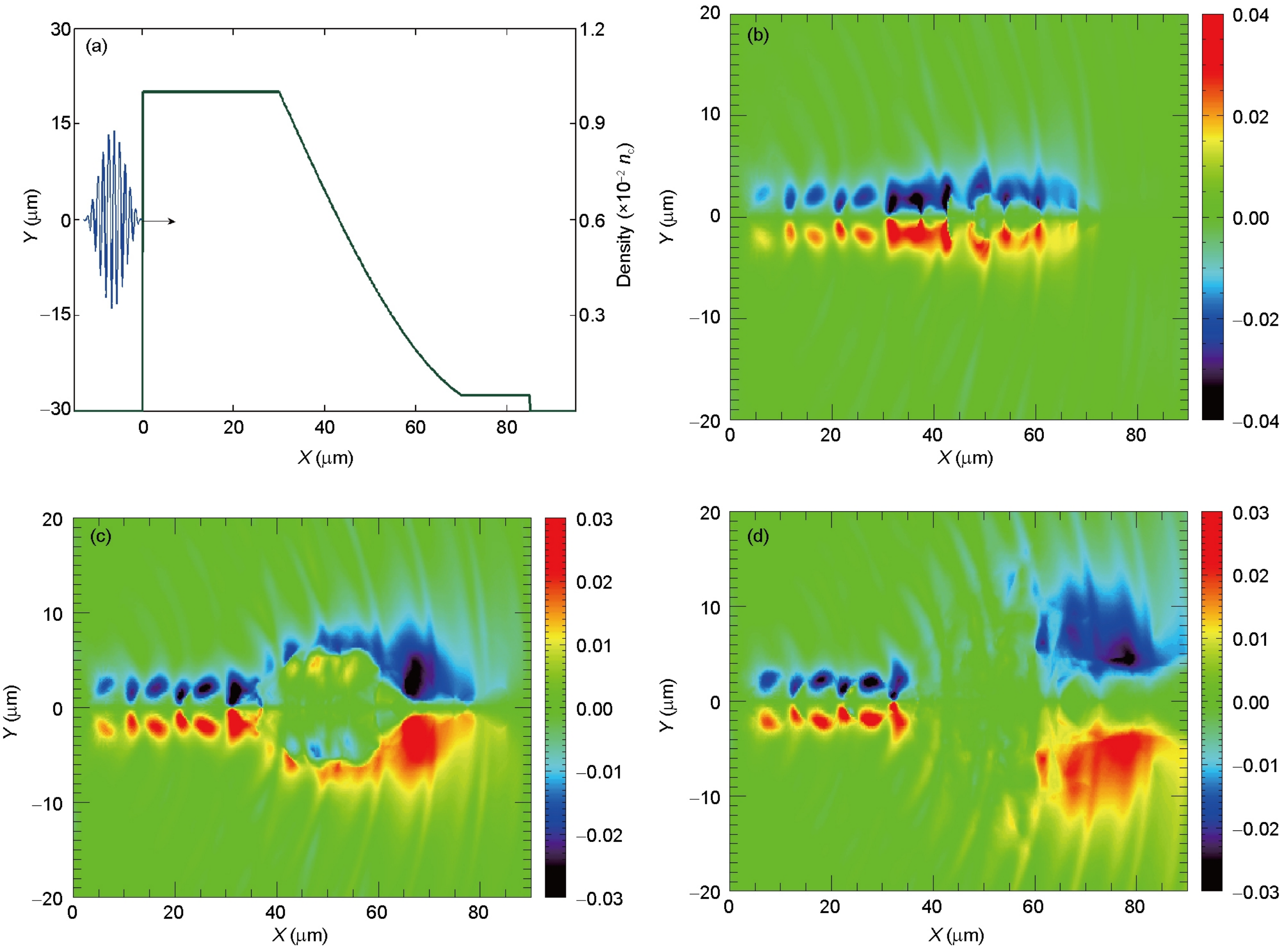

Figure 1 (Color online) 2D simulation results of the magnetic fields in the wake region. (a) Initial plasma density distribution and the laser profile along X direction; (b)-(d) the Z-component of the magnetic field (B_z) distribution at $108T_0$, $128T_0$, and $160T_0$, respectively. In this and following figures, the magnetic field and electric field are normalized by $B_N = m_e\omega_0 / 2\pi e = 1.7 \times 10^3 T$ and $E_N = m_e\omega_0 c / 2\pi e = 5.1 \times 10^{11}$ V/m, respectively.

by

$$I_0 = 1.37 \times 10^{18}\ \mathrm{W/cm^2}(\mu\mathrm{m}/\lambda_L)^2 a_0^2.$$

Absorbing boundary conditions are used for both particles and fields. Note that, compared with the work by Ping et al. [2] much lower laser intensity and plasma density have been used here. The mechanisms for magnetic field generation are completely different for the two cases.

Large-amplitude plasma waves are excited as an intense laser pulse propagates in underdense plasmas, due to the laser ponderomotive force both in the forward and side directions. With the resulting charge separation, the electrons oscillate around their equilibriums with a characteristic frequency roughly given by the electron plasma frequency. The source term of the quasi-static magnetic field on the right-hand side of eq. (2) points only along the Z direction in this 2D slab geometry. Figure 1(b)-(d) shows snapshots of the magnetic field component along this direction at different stages. In the homogeneous plasma region ($0 < X < 30$ μm), the magnetic field stays steady with time. It shows an oscillating component around $2k_p$ along the longitudinal direction, in addition to a uniform component which corresponds to a steady electric current driven by the laser pulse [21]. Here, k_p is the wave number of the plasma wave. The maximum strength of the magnetic field is about $0.05B_N$ or 1 MG under the given laser and plasma conditions.

In the plasma down-ramp region, however, rapid evolution of B_z is found, as presented in Figure 1(b)-(d). The magnetic field structure drifts rapidly in the lateral directions as well as longitudinally against the density gradient. The lateral drift is due to the force acting on the magnetic dipole vortex in the $\boldsymbol{B} \times \nabla \boldsymbol{n}$ direction according to refs. [22,23]. Note that this drift motion is completely different from the well-known diamagnetic drift [27]. Here, the electron magnetohydrodynamic fluid model is sufficient since the ion motion is negligible in this short period of time [28,29]. Interestingly, there are also opposite magnetic fields generated near the laser axis in the down-ramp, as shown in Figure 1(c). Up to t=$160T_0$, the drift is almost complete and the magnetic field fully gathers in the low-density plateau region with the peak spot at around x= 78 μm, where the initial magnetic fields right after laser passage are weak.

3 Magnetic field annihilation

Now we use two laser pulses, each with the same parameters defined above; they copropagate but are separated along the Y direction by 16 μm, with focal spot centers at $Y = \pm 8$ μm, respectively.

The evolution of the magnetic fields produced by the two laser pulses is shown in Figure 2(a), (c), and (e). Similarly, each pulse generates magnetic fields in its own wake. Mirrored by the center axis of the box, the magnetic fields show opposite polarities which will drift toward each other around the center in the plasma down-ramp. At t=108T_0, the magnetic fields in the low plateau are still negligible and the fields in the down-ramp have not yet drifted much, although the laser pulses have already propagated out of the box. Only 20T_0 later do the magnetic fields become largely accumulated on the right between X=60 and 80 μm, with significant transverse expansion. They start to overlap and annihilate near the central axis (Y=0). Full annihilation is achieved in another 30T_0 up to t=160T_0, as shown in Figure 2(e), while the outer fields have already drifted close to the box boundaries. Note that the annihilation of the magnetic fields results in the formation of inductive longitudinal electric fields near the central axis, as progressively depicted in Figure 2(b), (d), and (f). At the beginning right after the passage of the driving lasers in Figure 2(b), the longitudinal electric fields corresponding to charge separation are dominantly more intense in the high density regions, which is in line with the scaling of the wakefield strength with the plasma density, $E_x \propto n^{1/2}$. However, as the magnetic field drift occurs, the electric fields associated

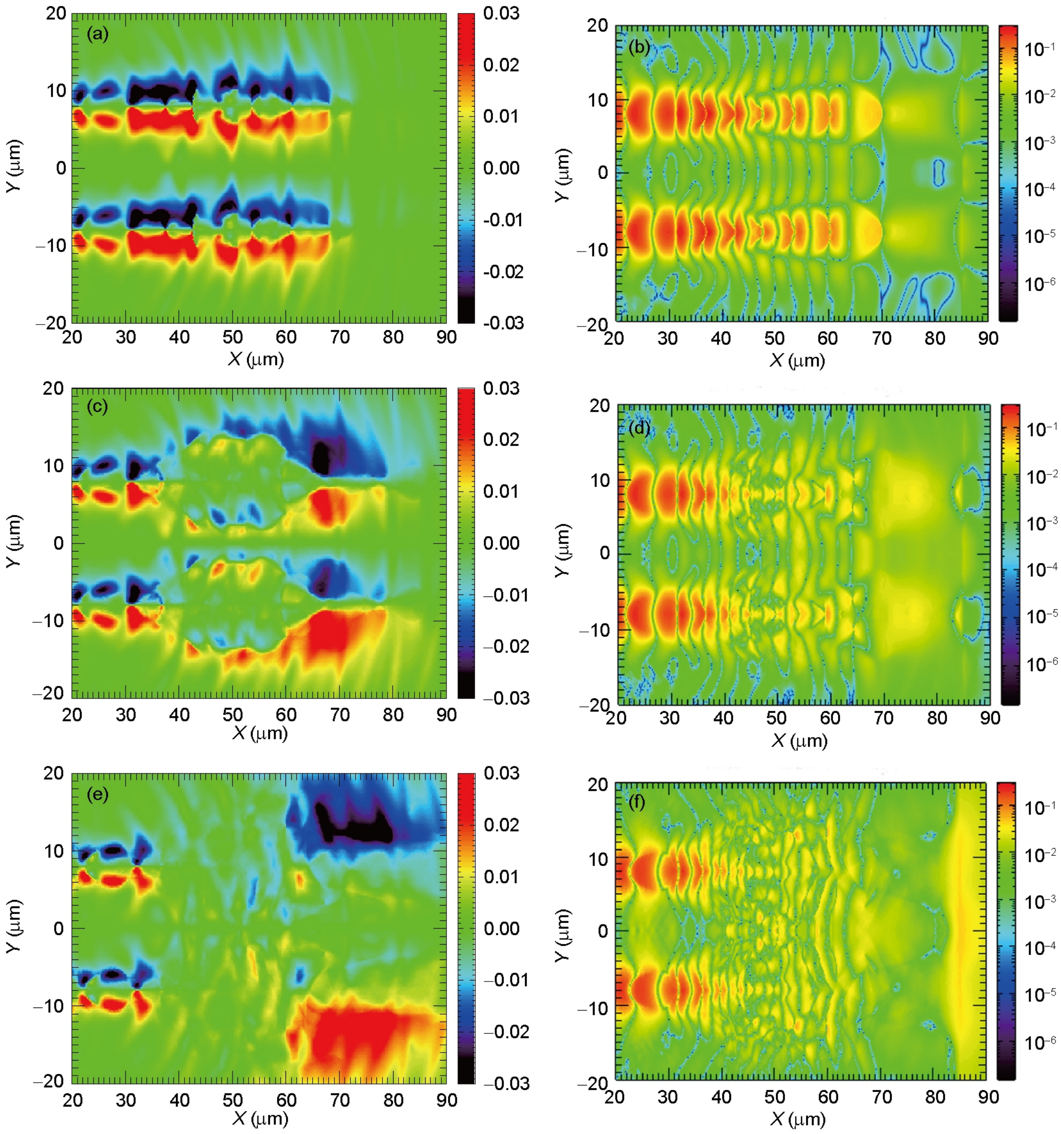

Figure 2 (Color online) 2D simulation results with two laser pulses. (a), (c), and (e) show the respective distributions of the Z-component of the magnetic field (B_z) at 108T_0, 128T_0 and 160T_0, respectively; (b), (d), and (f) show the corresponding absolute values of the electric field in the X direction ($|E_x|$) in logarithmic scale. The magnetic and electric fields are normalized as in Figure 1.

with the laser wakefield excitation weaken rapidly in the inhomogeneous region. At the same time, the rise of additional longitudinal electric fields around the central axis provides solid evidence of the magnetic field annihilation.

Figure 3(a) further shows the induced longitudinal electric field E_x near the magnetic field annihilation region at Y=0 at t=108T_0, 128T_0. Two consistent results are that E_x is mainly found in the nonuniform plasma region at the beginning free of annihilation and grows to substantial levels on the right around 70 μm $< X <$ 85 μm at t=128T_0, when the magnetic annihilation occurs. In addition, the ion skin depth is about d_i = 300 μm and the electron skin depth is about d_e = 7 μm in the low-density plateau region. The electron cyclotron is about 0.03ω_0 in both Figures 1 and 2. Because the magnetic annihilation occurs in a very short period of time, ion motion does not play a critical role. The averaged inductive electric field is about 0.01$E_{\rm N}$, which suggests that the magnetic field energy is efficiently converted to the electric field energy. The inductive electric fields generated in the annihilation region are unipolar and can accelerate charged particles. In this way, the magnetic field energy is again converted into the kinetic energy of plasma. Here, the inductive electric field represented by the E_x component is positive according to the generalized Ohm's law [2,17,30]; therefore, it accelerates electrons in the negative direction of the X-axis.

We present the electron momentum distribution in Figure 3(b)-(d) for the three instances described so far. At t=108T_0, most electrons have only small momenta because few electrons are trapped and accelerated by the laser wakefield under the given laser and plasma conditions. A few electrons have positive velocities along the X direction, mainly due to electron acceleration by the laser ponderomotive force. However, at t=160T_0, a large number of electrons are accelerated considerably along the negative X direction. Obviously, they are accelerated by the inductive electric fields pointing along the positive X-axis. During the magnetic annihilation, electrons are mainly accelerated by the longitudinal electric fields, even though their transverse momenta are increased, due to the presence of transverse magnetic and electric fields.

4 Magnetic reconnection

In order to check the 3D effects, we also carried out 3D simulations in $L_x \times L_y \times L_z$ = 115 μm×60 μm×50 μm simulation box, divided into 3450×600×500 cells. All the laser plasma conditions are the same as above, with uniform density along the third direction.

The most noticeable differences between the 3D and 2D simulations are that the self-generated magnetic fields become azimuthal around the laser axis in the 3D examples, in contrast to Z-polarized in the 2D slab geometry. In the density down-ramp region, quasi-static magnetic fields expand radially and magnetic reconnection occurs when the expanding magnetized plasma bubbles meet each other around the box

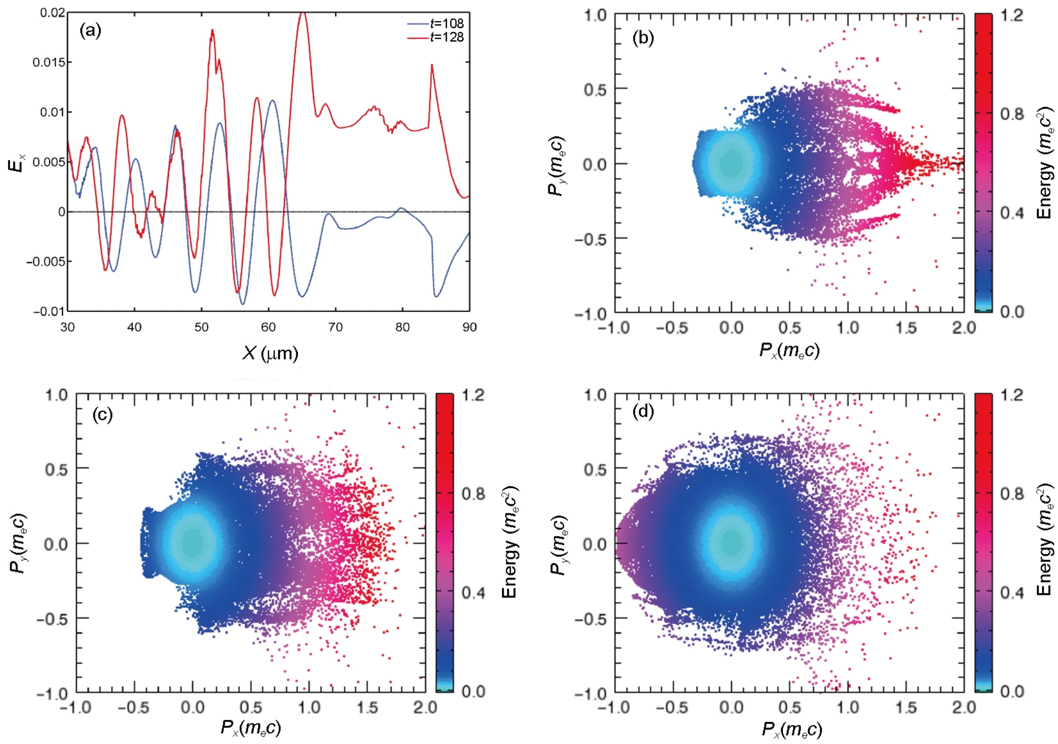

Figure 3 (Color online) (a) Longitudinal electric fields E_x along the central axis (Y=0) at 108T_0 and 128T_0, respectively; (b)-(d) show the respective electron momentum distributions at 108T_0, 128T_0 and 160T_0; where the color bars represent the particle kinetic energy.

center. This is illustrated in Figure 4 by transverse cuts of the magnetic fields at $X = 65$ μm for t=108T_0 to 120T_0. In Figure 4(a) and (b), we only present the Z-component of the magnetic fields, B_z, which have double-lobe profiles for each wake. Bear in mind that they are azimuthal, so the magnetic fields should be annular-like, with the Y-components having similar profiles but aligned in the orthogonal direction. This result is more evident in Figure 4(c) and (d) in terms of vector plots. At t=108T_0, the distance between the centers of the two magnetic dipoles is about 4 μm, which means the two bubbles have expanded but have not yet squeezed each other dramatically. As the field drift continues, the magnetic fields gradually converge around the box center and form a reconnection X-line at the leading point of tangency (namely, at $Y = 0$) between the bubbles. As shown in Figure 4(d), the two magnetic bubbles reconnect in the outer region at t=120T_0. When the magnetic fields with different polarities meet at the diffusion region, the field annihilation develops. As the field structures are rearranged, an electric field perpendicular to the plane is derived.

Figure 5 shows the electric field in the 3D simulation. At the X-Z plane ($Y = 0$), magnetic reconnection occurs dramatically and derives an electric field, which will accelerate electrons to high speed. Figure 5(a) and (c) presents the electric field at 108T_0. At this moment, some of the magnetic field has already been rearranged and induces a positive electric field along the X direction. This result explains why the peak field value is bigger than the valley value. Between 70 μm $< X <$ 85 μm, the initial density is almost zero and the E_x is along the positive X direction, which indicates that magnetic reconnection dominates the electric field. At t=120T_0, the periodicity of E_x is destroyed and the maximum amplitude is about 0.01$E_{\rm N}$. This is when magnetic reconnection occurs most dramatically in the Y-Z plane (X=65). At the same time, the reconnection-induced electric fields effectively heat the plasma electrons to convert a portion of the magnetic energy to kinetic energy. These energetic electrons may further be diverted by the Hall effect, leading to hot electron jets in the annihilation plane (Figure 6).

The momentum space of electrons in −4 μm<Y<4 μm is illustrated in Figure 6 at 108T_0 and 160T_0. At t=108T_0, most of the electrons with small momentum gather around zero. After 52T_0, when the magnetic reconnection is almost complete, the X-component momentum of electrons increases; this means the particles are accelerated by the inductive electric field, as shown in Figure 6(c). Figure 6(d) also shows that both the Y-component and Z-component momentum are increased. This increase in the number of energetic particles confirms that magnetic energy is converted to kinetic energy by the reconnection process.

One of the most important issues in the magnetic reconnection process is the reconnection (annihilation) rate $E_{\rm R} / BV_{\rm A}$, where $E_{\rm R}$ is the inductive electric field and $V_{\rm A}$ is the Alfven speed evaluated by both plasma density and magnetic field. We calculated the rate in the plateau region (70 μm $< X <$ 85 μm) where magnetic fields gather together

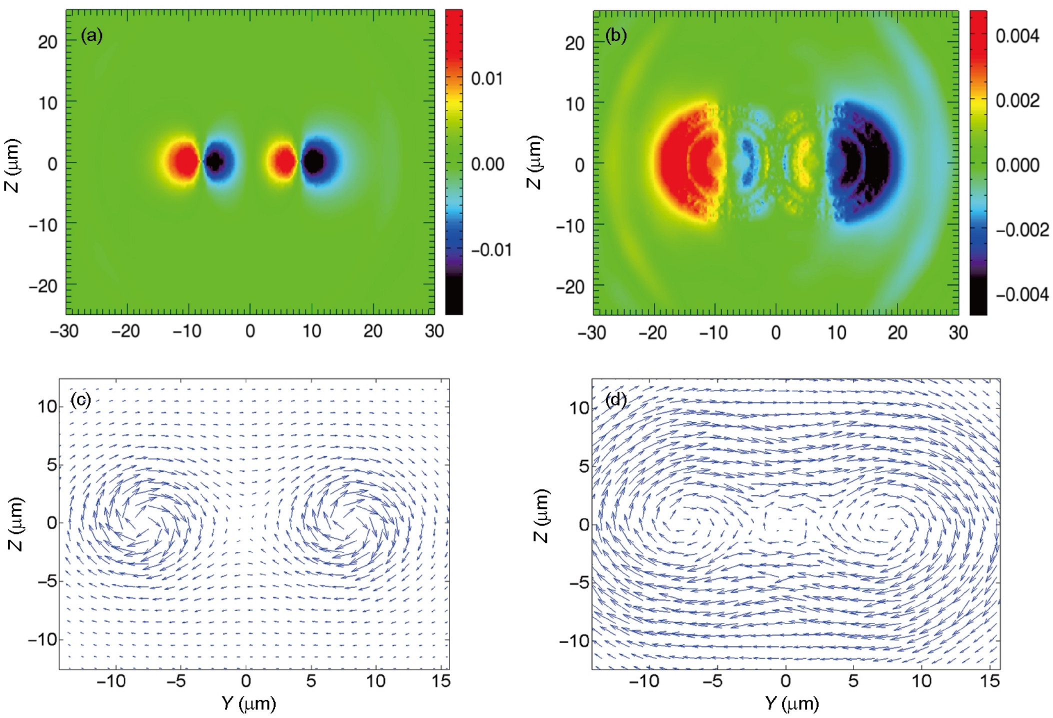

Figure 4 (Color online) 3D simulation results with two laser pulses. (a) and (b) show the respective distributions of the Z-component magnetic field (B_z) in the Y-Z plane at $X = 65$ μm at 108T_0 and 120T_0, respectively; (c) and (d) respectively show the corresponding magnetic field vectors (B_y, B_z) in the plane at 108T_0 and 120T_0. The arrows indicate the direction and strength of the magnetic fields.

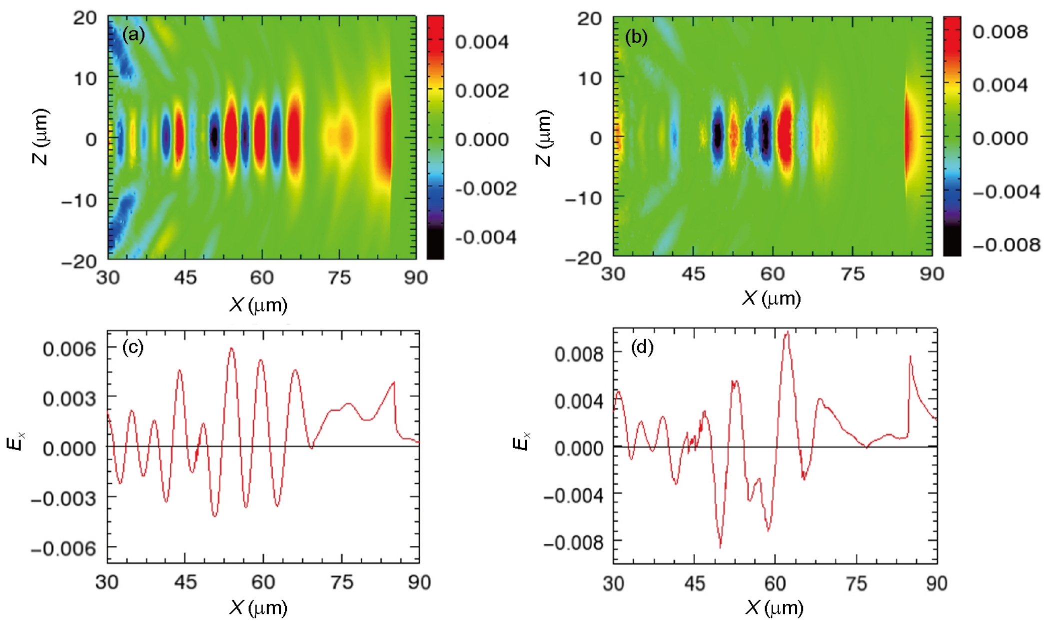

Figure 5 (Color online) (a) and (b) the longitudinal electric field E_x in the X-Z plane (at Y=0) at $108T_0$ and $120T_0$; (c) and (d) the corresponding E_x along the X-axis (Y=0, Z=0).

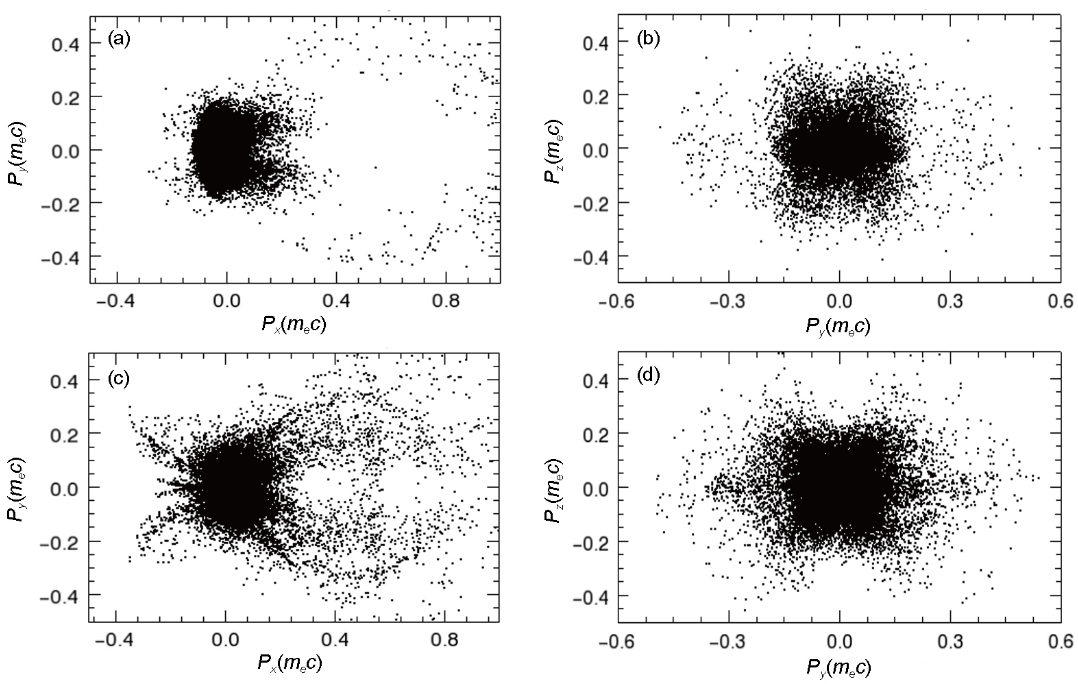

Figure 6 The momentum space of electrons between -4 μm $< Y <$ 4 μm. (a) and (c) show electron momentum spaces (P_x, P_y) at $108T_0$ and $160T_0$; (b) and (d) show electron momentum spaces (P_y, P_z) at $108T_0$ and $160T_0$.

and annihilate. In 2D simulations, the magnetic field $B = 0.03B_N = 51T$; the inductive electric field $E_R = 0.01E_N = 51\times10^9$ V/m, the plasma density $n = 5.658\times10^{17}$ cm$^{-3} = 5\times10^{-4}n_c$; and the corresponding Alfven speed $V_A = 1.48\times10^6$ m/s, about 1/200 of the light speed, which results in a reconnection rate of E_R/BV_A =67.6. In comparison, the magnetic field and electric field are $B = 0.015B_N = 25.5T$ and $E_R = 0.002E_N = 1.02\times10^9$ V/m in 3D simulations. The Alfven speed is estimated to be $V_A = 7.39\times10^5$ m/s and reconnection rate is E_R/BV_A = 54.1. Here we have used the density and magnetic field conditions when the magnetic reconnection starts to develop. The rates in both 2D and 3D simulations are much larger than the typical value 0.1 obtained by MHD simulations for Hall magnetic reconnection [31]. This increase indicates a prominent feature of this system of underdense plasmas driven by intense short-pulse lasers.

5 Summary

We studied magnetic field drift in inhomogeneous plasmas driven by ultrashort intense laser pulses, and the consequent magnetic reconnection of two copropagating pulses with close spot deviations. In the plasma wake behind the laser pulses, high-order electron fluid nonlinearities created intense quasi-static magnetic fields, which drifted rapidly in the forward and lateral directions in a density down-ramp plasma. When the magnetic fields with different polarities drifted toward each other and annihilated at the diffusion region, electric fields were effectively induced, resulting in significant electron heating. At the same time, hot electron jets in the diffusion region were generated, which is one of the signature events that prove the energy conversion from magnetic field to kinetic energy. The reconnection rate found in the simulation was much larger than the typical value obtained in Hall magnetic reconnection, providing clear evidence of fast reconnection. Our work suggests a way for experimental realization of fast magnetic reconnection with intense short laser pulses of terawatt peak power only.

This work was supported by the National Basic Research Program of China (Grant No. 2013CBA01500), the National Natural Science Foundation of China (Grant Nos. 11421064, and 11220101002), and a Leverhulme Trust Research Project Grant at University of Strathclyde.

1 M. Yamada, Phys. Plasmas **14**, 058102 (2007).
2 Y. L. Ping, J. Y. Zhong, Z. M. Sheng, X. G. Wang, B. Liu, Y. T. Li, X. Q. Yan, X. T. He, J. Zhang, and G. Zhao, Phys. Rev. E **89**, 031101 (2014).
3 J. Zhong, Y. Li, X. Wang, J. Wang, Q. Dong, C. Xiao, S. Wang, X. Liu, L. Zhang, L. An, F. Wang, J. Zhu, Y. Gu, X. He, G. Zhao, and J. Zhang, Nat. Phys. **6**, 984 (2010).
4 E. N. Parker, J. Geophys. Res. **62**, 509 (1957).
5 J. B. Taylor, Rev. Mod. Phys. **58**, 741 (1986).
6 Q. L. Dong, S. J. Wang, Q. M. Lu, C. Huang, D. W. Yuan, X. Liu, X. X. Lin, Y. T. Li, H. G. Wei, J. Y. Zhong, J. R. Shi, S. E. Jiang, Y. K. Ding, B. B. Jiang, K. Du, X. T. He, M. Y. Yu, C. S. Liu, S. Wang, Y. J. Tang, J. Q. Zhu, G. Zhao, Z. M. Sheng, and J. Zhang, Phys. Rev. Lett. **108**, 215001 (2012), arXiv: 1203.4036.
7 P. M. Nilson, L. Willingale, M. C. Kaluza, C. Kamperidis, S. Minardi, M. S. Wei, P. Fernandes, M. Notley, S. Bandyopadhyay, M. Sherlock, R. J. Kingham, M. Tatarakis, Z. Najmudin, W. Rozmus, R. G. Evans, M. G. Haines, A. E. Dangor, and K. Krushelnick, Phys. Plasmas **15**, 092701 (2008).
8 X. X. Pei, J. Y. Zhong, Y. Sakawa, Z. Zhang, K. Zhang, H. G. Wei, Y. T. Li, Y. F. Li, B. J. Zhu, T. Sano, Y. Hara, S. Kondo, S. Fujioka, G. Y. Liang, F. L. Wang, and G. Zhao, Phys. Plasmas **23**, 032125 (2016).
9 R. L. Richard, R. D. Sydora, and M. Ashour-Abdalla, Phys. Fluids B-Plasma Phys. **2**, 488 (1990).
10 W. Fox, A. Bhattacharjee, and K. Germaschewski, Phys. Plasmas **19**, 056309 (2012).
11 C. K. Li, F. H. Séguin, J. A. Frenje, J. R. Rygg, R. D. Petrasso, R. P. J. Town, O. L. Landen, J. P. Knauer, and V. A. Smalyuk, Phys. Rev. Lett. **99**, 055001 (2007).
12 M. G. Haines, Phys. Rev. Lett. **78**, 254 (1997).
13 X. G. Wang, C. J. Xiao, Z. Y. Pu, and J. Q. Wang, Chin. Sci. Bull. **57**, 1369 (2012).
14 K. Huang, C. Huang, Q. Dong, Q. Lu, S. Lu, Z. Sheng, S. Wang, and J. Zhang, Phys. Plasmas **24**, 041406 (2017).
15 S. Lu, Q. Lu, C. Huang, Q. Dong, J. Zhu, Z. Sheng, S. Wang, and J. Zhang, New J. Phys. **16**, 083021 (2014).
16 S. Lu, Q. Lu, F. Guo, Z. Sheng, H. Wang, and S. Wang, New J. Phys. **18**, 013051 (2016).
17 Y. J. Gu, O. Klimo, D. Kumar, S. V. Bulanov, T. Z. Esirkepov, S. Weber, and G. Korn, Phys. Plasmas **22**, 103113 (2015).
18 Y. J. Gu, Q. Yu, O. Klimo, T. Z. Esirkepov, S. V. Bulanov, S. Weber, and G. Korn, High Pow Laser Sci. Eng. **4**, e19 (2016).
19 Y. Q. Cui, Z. M. Sheng, Q. M. Lu, Y. T. Li, and J. Zhang, Sci. China-Phys. Mech. Astron. **58**, 105201 (2015), arXiv: 1506.00049.
20 S. Mondal, V. Narayanan, W. J. Ding, A. D. Lad, B. Hao, S. Ahmad, W. M. Wang, Z. M. Sheng, S. Sengupta, P. Kaw, A. Das, and G. R. Kumar, Proc. Natl. Acad. Sci. **109**, 8011 (2012).
21 Z. M. Sheng, J. Meyer-Ter-Vehn, and A. Pukhov, Phys. Plasmas **5**, 3764 (1998).
22 S. K. Yadav, A. Das, and P. Kaw, Phys. Plasmas **15**, 062308 (2008), arXiv: 0804.3934.
23 J. Nycander, and M. B. Isichenko, Phys. Fluids B-Plasma Phys. **2**, 2042 (1990).
24 T. Tajima, and J. M. Dawson, Phys. Rev. Lett. **43**, 267 (1979).
25 Z. M. Sheng, K. Mima, Y. Sentoku, K. Nishihara, and J. Zhang, Phys. Plasmas **9**, 3147 (2002).
26 R. A. Fonseca, L. O. Silva, F. S. Tsung, V. K. Decyk, W. Lu, C. Ren, W. B. Mori, S. Deng, S. Lee, T. Katsouleas, and J. C. Adam, in *Lecture Notes in Computer Science: Proceedings of International Conference on Computational Science (ICCS) 2002* (Springer, Berlin, Heidelberg), 2331: 342-351.
27 F. F. Chen, *Introduction to Plasma Physics and Controlled Fusion, 2nd ed* (Plenum Press, New York, 1984).
28 Q. M. Lu, R. S. Wang, J. L. Xie, C. Huang, S. Lu, and S. Wang, Chin. Sci. Bull. **56**, 1174 (2011).
29 J. Guo, Chin. Sci. Bull. **54**, 456 (2009).
30 H. Che, J. F. Drake, and M. Swisdak, Nature **474**, 184 (2011).
31 J. D. Huba, and L. I. Rudakov, Phys. Rev. Lett. **93**, 175003 (2004).